(2)

ARMY RESEARCH LABORATORY

A Parametric Investigation of Muzzle Blast

Kevin S. Fansler
William P. Thompson
John S. Carnahan
Brendan J. Patton

ARL-TR-227 September 1993

NOTICES

Destroy this report when it is no longer needed. DO NOT return it to the originator.

Additional copies of this report may be obtained from the National Technical Information Service, U.S. Department of Commerce, 5285 Port Royal Road, Springfield, VA 22161.

The findings of this report are not to be construed as an official Department of the Army position, unless so designated by other authorized documents.

The use of trade names or manufacturers' names in this report does not constitute indorsement of any commercial product.

REPORT DOCUMENTATION PAGE

Form Approved
OMB No 0704-0188

1. AGENCY USE ONLY (Leave blank)	2. REPORT DATE	3. REPORT TYPE AND DATES COVERED
	September 1993	Final, October 1991 - September 1992

4. TITLE AND SUBTITLE

A PARAMETRIC INVESTIGATION OF MUZZLE BLAST

5. FUNDING NUMBERS

PR: 1L161102AH43
WO: 61102A-00-001 AJ

6. AUTHOR(S)

KEVIN S. FANSLER, WILLIAM P. THOMPSON, JOHN S. CARNAHAN, and BRENDAN J. PATTON

7. PERFORMING ORGANIZATION NAME(S) AND ADDRESS(ES)

US Army Research Laboratory
ATTN: AMSRL-WT-PB
Aberdeen Proving Ground, MD 21005-5066

8. PERFORMING ORGANIZATION REPORT NUMBER

9. SPONSORING / MONITORING AGENCY NAME(S) AND ADDRESS(ES)

US Army Research Laboratory
ATTN: AMSRL-OP-CI-B (Tech Lib)
Aberdeen Proving Ground, Maryland 21005-5066

10. SPONSORING / MONITORING AGENCY REPORT NUMBER

ARL-TR-227

11. SUPPLEMENTARY NOTES

This report supersedes BRL-IMR-974, September 1992.

12a. DISTRIBUTION / AVAILABILITY STATEMENT

Approved for public release; distribution is unlimited.

12b. DISTRIBUTION CODE

13. ABSTRACT *(Maximum 200 words)*

Weapons that vary greatly in their bore lengths are fired over a wide range of projectile velocities. Pressure transducers are located from 15 to 400 calibers from the muzzle and at 30-degree increments around the gun. The investigation yields a detailed picture of the flow field, as displayed by overpressure traces. Comparisons of the overpressure data with an older established prediction method show better agreement for the measured points nearer to the muzzle. Here, a scaling approach combined with a parametric least squares investigation is used to model the peak overpressure, which asymptotically approaches the far field behavior, yet gives the nonlinear behavior nearer the muzzle. Using the shock wave expression, which depends on the fitted peak overpressure results, an expression for the time of arrival is obtained which in turn is fitted to the time of arrival data. The positive phase duration is then obtained by subtracting the time of arrival from the zero pressure point of the wave, which is traveling at the approximate speed of sound. The shape of the positive phase of the wave is then assumed to correspond to a Friedlander wave. Assuming the shape, an expression for the impulse of the positive phase is obtained that depends on the fitted peak overpressure and the value of the positive phase duration. The parameters describing the positive phase duration are then fitted by using the impulse data. In summation, the physics of the blast wave is used to construct the time of arrival, positive phase duration, and impulse models.

14. SUBJECT TERMS

fluid dynamics; impulse noise; muzzle blast; noise management; overpressure

15. NUMBER OF PAGES

36

16. PRICE CODE

17. SECURITY CLASSIFICATION OF REPORT	18. SECURITY CLASSIFICATION OF THIS PAGE	19. SECURITY CLASSIFICATION OF ABSTRACT	20. LIMITATION OF ABSTRACT
UNCLASSIFIED	UNCLASSIFIED	UNCLASSIFIED	UL

INTENTIONALLY LEFT BLANK.

TABLE OF CONTENTS

INTENTIONALLY LEFT BLANK.

LIST OF FIGURES

INTENTIONALLY LEFT BLANK.

LIST OF TABLES

INTENTIONALLY LEFT BLANK.

Acknowledgment

We wish to thank Mr. Donald McClellan for his invaluable assistance with the experiments. We also wish to thank Mr. Gordon Brown and Mr. David Webb for their valuable comments.

INTENTIONALLY LEFT BLANK.

1. INTRODUCTION

1.1 Background. There is a need to predict blast wave overpressure levels accurately over a large range of distances from the gun muzzle. For instance, designing an enclosure for reducing impulsive noise requires an estimate of the forces and impulses on its inside surfaces. The enclosure's walls, which reduce noise emanating from large guns, may be as far away as 100 calibers from the gun muzzle. But it is also important to know muzzle-blast levels closer to the gun. Muzzle blast can injure people and harm material at shorter ranges. It is therefore important to be able to predict blast levels for new or upgraded weapons before they are fired to avoid unexpected damage.

The muzzle blast levels depend on the weapon design and emplacement, the propellant and projectile characteristics, and the launch conditions. By generalizing and extending Smith's work (1974), the U.S. Army Research Laboratory (formerly the Ballistic Research Laboratory [BRL]) developed prediction methods for bare muzzle guns based on data collected in the range of 10 to 50 calibers from the gun muzzle (Fansler & Schmidt 1983; Fansler 1985; Heaps, Fansler, & Schmidt 1985). This approach was also based on the coupling between solutions to the problems of variable energy blast waves and blast waves from asymmetrically initiated charges. From dimensional analysis (Baker 1973), a scaling length, ℓ', is obtained. This scaling length depends on such parameters as the exit muzzle pressure, exit temperature of the propellant, and the field angular position from the gun bore axis. The field distance from the muzzle divided by a scaling length is used as the universally independent variable to plot the peak overpressure, and so forth. Free parameters are generated by the dimensional analysis and are determined by a least squares fit to the data. The resultant predicted free field muzzle blast is implemented on a computer and can be applied for blast waves incident on surfaces to obtain the reflected pressures.

In the studies cited above, data were collected for distances close to the muzzle. The larger distances encountered for the enclosure generate an uncertainty about the prediction accuracy (especially the impulse). Although the old model predicts impulse and peak overpressures close to the muzzle, an examination of the impulse expression shows the energy of the wave is increasing although it should decrease with larger distances. Other people have investigated muzzle blast at greater distances. Soo Hoo and Moore (1972) primarily studied various naval guns with data taken for distances between 20 and 110 calibers. They obtained pressure contours scaled in terms of calibers for naval guns with bore sizes from 40 mm to 8 inch (203 mm). They also obtained data for U. S. Army 20-mm M3 and M197 cannon. Naval guns of different bore diameters but having the same barrel length in calibers scaled well over a large range of distances. Scaling for the naval guns was achieved even though

the distance in calibers from the ground plane to the muzzle was not constant.

Pater (1981) obtained additional data in the far field for naval guns. Using Soo Hoo and Moore's data, he investigated the changing relative angular distribution of the gun blast's shock wave strength with distance. The peak sound pressure level (PSPL) was approximately 23 dB greater at the front than at the rear for the pressure wave front located 20 calibers from the muzzle of a 5-inch/54 naval gun, while in the far field, the PSPL difference decreased to 14.3 dB. Schomer, Little, and Hunt (1979) used guns ranging from mortars to tank cannon to obtain PSPL differences ranging from 14 to 18 dB in the far field. Most recently, Kietzman, Fansler, and Thompson (1991) have obtained data from a 105-mm tank cannon and noted that the angular distribution of the shock wave strength changed with distance. The original model of Fansler and Schmidt (1983) assumed an unchanging distribution with distance.

1.2 Objectives. It is the purpose of this investigation to develop a model for muzzle blast that accurately predicts quantities for a large range of distances from the muzzle. The physics of the blast wave are to be emphasized while constructing the model, which uses a scaling approach with free parameters to be fit with the experimental results. To these ends, data are obtained using a wide variety of weapon parameters using a large range of distances to provide an adequate data base for the improved model.

2. EXPERIMENTAL SETUP

The experiment to obtain the small caliber data was conducted at the ARL indoor aerodynamics range for distances 15 to 100 calibers from the muzzle. Because of limited space in the indoor aerodynamics range, the ARL transonic range was used when the gauges were placed 400 calibers from the muzzle. The weapons used in the test were a 300-magnum barrel, another 300-magnum barrel that had a reduced bore length, and a shortened carbine barrel. A schematic of the gauge positions around the gun muzzles is shown in Figure 1. In addition, a gauge was positioned near the muzzle to establish a zero reference time for the experiment. The current small caliber data were supplemented by 105-mm tank cannon data obtained in the Kietzman, Fansler, and Thompson (1991) experiment.

The loadings, velocity, and muzzle pressure are shown in Table 1. The muzzle pressure in the last column is the peak value just before the projectile exits the barrel. With the exception of the last row, the first number in the description column of Table 1 refers to the projectile mass in grains, while the second number refers to the charge mass in grains. Further discussions about the firings will use these descriptions for identification. The last

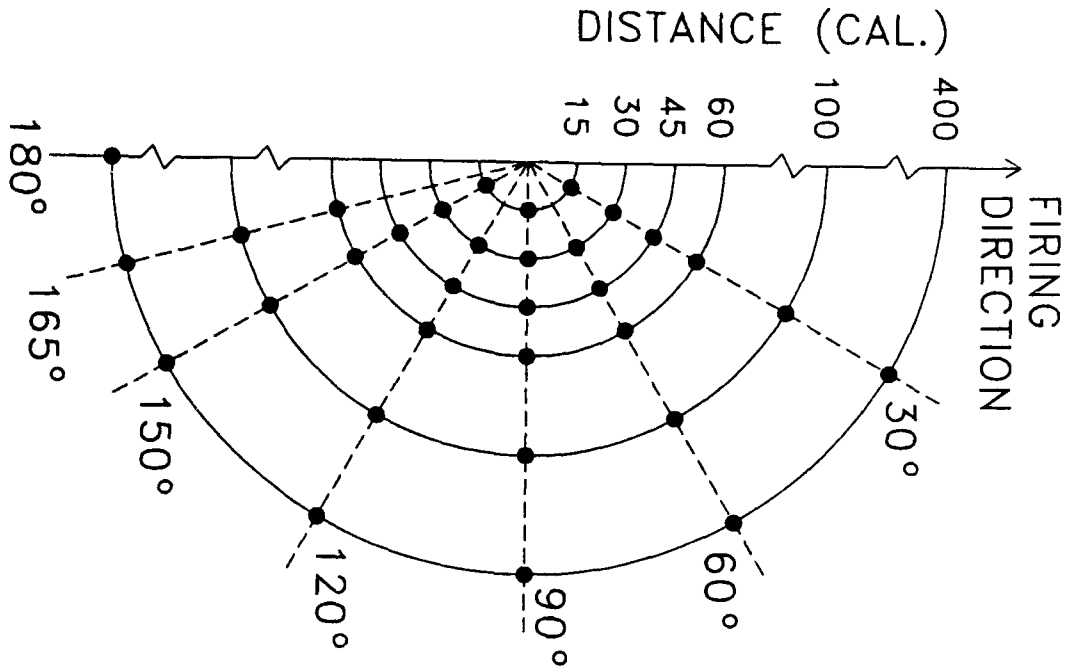

Figure 1. Gauge Positions for Study

row refers to the parameters for the 105-mm cannon shooting the M735 round.

3. MODELING APPROACH

The authors predict four quantities that partially characterize the blast wave. Three of these quantities are illustrated in Figure 2. The peak overpressure, $\bar{P} \equiv (p_p - p_\infty)/p_\infty$, is shown as is the time of arrival, t_a, and the positive phase duration, τ. The time of arrival is simply the time elapsed between the projectile exiting the muzzle and the arrival of the wave at the selected field point. The positive phase duration is the time difference between the passage of the wave front and the passage of the wave's change from positive overpressure to negative overpressure. The impulse corresponding to the time integral of the wave's positive phase is also of interest.

For gun muzzle blast, the energy efflux from the muzzle declines monotonically. For instantaneous energy deposition, dimensional analysis leads to scaling relationships that generate universal curves. Gun blast can be treated in a similar manner but in place of the instantaneous energy, E, the peak energy efflux, dE/dt, is used. The peak overpressure, $P \equiv p_p - p_\infty$, is expressed in functional terms as,

$$P = P(r, \rho_\infty, a_\infty, dE/dt), \tag{1}$$

Table 1. Loadings and Characteristics

Barrel	Description	Propellant Type	Charge Mass g	(gr)	Projectile Velocity m/s	(ft/s)	Muzzle Pressure MPa	(kpsi)
300 Long Magnum	l220w70	4831	4.82	(70.0)	899	(2950)	59.40	(8.62)
	l220w12	Bullseye	0.83	(12.0)	282	(925)	15.56	(2.26)
	l125w75	4831	5.16	(75.0)	975	(3200)	80.65	(11.69)
	l125w12	Bullseye	0.83	(12.0)	457	(1500)	20.37	(2.95)
300 Short Magnum	s220w36	4227	2.48	(36.0)	594	(1950)	74.9	(10.85)
	s220w9	Bullseye	0.62	(9.0)	221	(725)	17.7	(2.57)
	s125ws42	4227	2.89	(42.0)	792	(2600)	89.60	(12.99)
Carbine	c13p6	2400	0.94	(13.6)	518	(1700)	6.59	(9.56)
105 mm	105mm	M30	5966	(-)	1501	(4925)	71.5	(10.37)

in which

p_p = peak value of the pressure at a given field point,

r = distance from muzzle to field point,

ρ_∞ = ambient density,

a_∞ = ambient speed of sound,

dE/dt = energy deposition rate into atmosphere.

Here the energy deposition rate can be written as,

$$\frac{dE}{dt} = \frac{\gamma_e p_e u_e}{\gamma_e - 1}[1 + \frac{(\gamma_e - 1)}{2} M_e{}^2] A_e \tag{2}$$

in which A_e is the area of the bore, M_e is the exit Mach number of the propellant flow immediately after the projectile exits the muzzle, $\bar{p}_e$ is the peak muzzle pressure divided by the atmospheric pressure, u_e is the velocity of the exiting propellant, and γ_e is the specific heat ratio for the exiting propellant. For supersonic flow the exit conditions would be identical to the conditions just before projectile release from the muzzle. For subsonic flow the exit conditions are different and are discussed by Fansler and Schmidt (1983).

Using the Buckingham Pi theorem, a scaling length for constant energy efflux explosion is obtained,

$$\ell \sim \sqrt{(dE/dt)/(p_\infty a_\infty)} \tag{3}$$

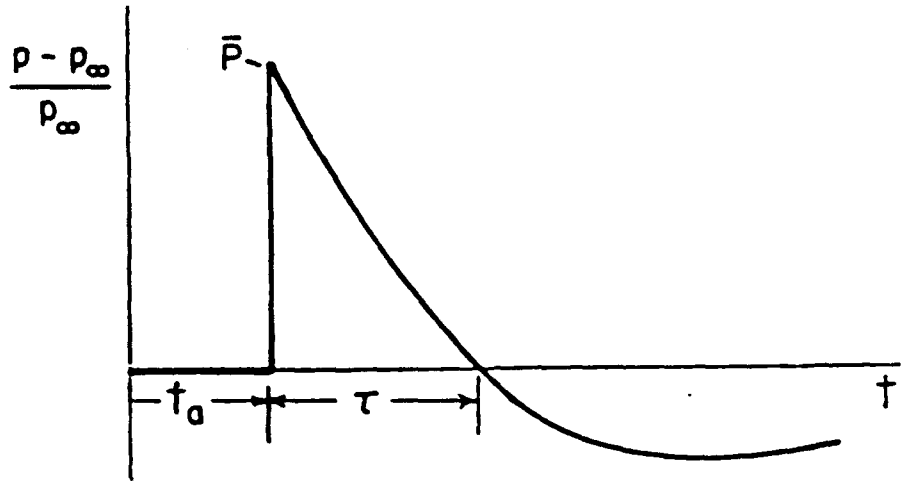

Figure 2. Blast Wave Values to be Obtained

and

$$\bar{P} \equiv P/p_\infty = \bar{P}(r/\ell). \tag{4}$$

Also the time of arrival, t_a, and the positive phase duration, τ, scale as

$$t_a a_\infty/\ell = f(r/\ell), \tag{5}$$

and,

$$\tau a_\infty/\ell = g(r/\ell). \tag{6}$$

The above treatment, which assumes spherically symmetrical conditions, is modified for gun blast, where the peak overpressure varies strongly with the polar angle, θ, from the boreline. Following Smith (1974), we obtain a scaling length, ℓ', that depends on the polar angle,

$$\ell'/\ell = \mu\cos\theta + \sqrt{1-\mu^2\sin^2\theta}, \tag{7}$$

in which μ is the momentum index, which determines the ratio of the peak overpressure (with distance held constant) to the front along the boreline divided by the peak overpressure to the rear along the boreline. With the modification, we have for the gun blast peak overpressure,

$$\bar{P} = \bar{P}(\bar{r}), \tag{8}$$

in which $\bar{r} \equiv r/\ell'$.

3.1 Peak Overpressure. Before, we assumed a one-term equation that was fitted with the data to obtain the value of μ and the exponent power of $\bar{r}$. That is, $\bar{P}(0°)/\bar{P}(180°)$ did not vary with the distance from the muzzle. But here, a nonlinear equation is assumed so that the above ratio of peak overpressures changes with distance from the muzzle. The predictive expression models an acoustic wave at large distances but closer in the peak overpressure versus distance relationship has a steeper slope, as also occurs with instantaneous explosions. The following expression for the peak overpressure, $\bar{P}$, is assumed:

$$\bar{P} = \frac{A}{\bar{r}} + \frac{B}{\bar{r}^2}. \tag{9}$$

Equation (9) is matched with pressure data and, as before, uses Equation (7) to vary the strength of the blast with the polar angle, θ.

Originally, we used Equation (9) with the data obtained in the far field to obtain the value of the momentum index. The dependence of the blast strength with angle would thus be well established in the far field. The values of A and B could then be determined by least squares fitting with both the near and far field data. Since it is well known that the value of μ in the far field depends on a particular weapon, significant parameters were sought for the blast strength dependence on angle.

One candidate is the blow-down parameter, δ, which is essentially the ratio of the scales for the gun tube emptying time and the time scale for the muzzle blast

$$\delta = \frac{La_\infty}{V_p \ell}, \tag{10}$$

in which L is the length of the gun barrel in calibers, a_∞ is the ambient sound speed, and V_p is the muzzle velocity of the projectile. Fansler and Schmidt (1983) used a numerical code developed by Erdos and DelGuidice (1975) to establish the dependence of the peak overpressure upon δ. Figure 3 shows how the peak overpressure varies with barrel length, which is equivalent to varying δ. Guided by the results of the Erdos code, Fansler (1985) found that the measured positive phase duration and impulse descriptions could be improved by including the parameter, $\beta \equiv \delta\ell/\ell'$, into the least squares fitting. The parameter β has the same meaning as δ except now, the angular position of interest is taken into account.

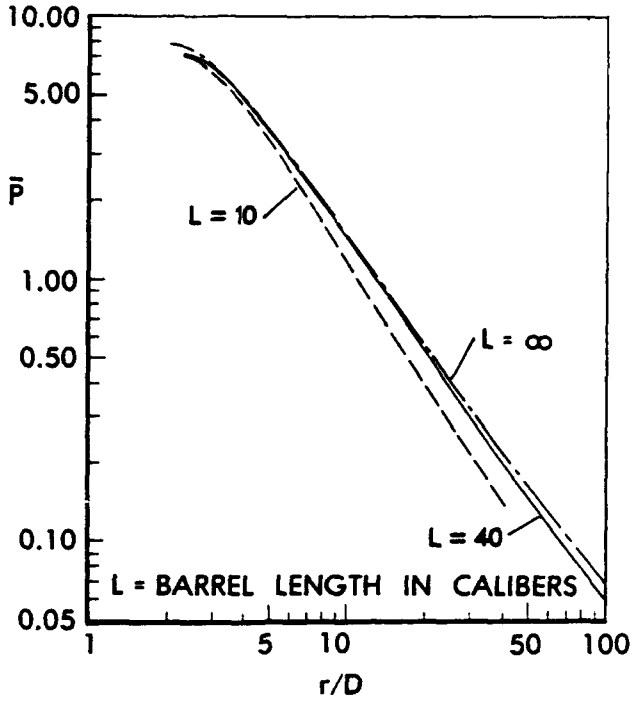

Figure 3. Variation of Peak Overpressure with Barrel Length

The location of the Mach disc is also used as a parameter to fit the dependence of blast strength on the angle as is the scale length ℓ/D in which D is the diameter of the bore. The authors also used an apparent source point for the gun blast, which is forward of the muzzle at a fixed fraction of the distance from the muzzle to the Mach disc for an equivalent steady jet. Shadowgraphs of the blast wave show an almost spherical structure whose center is forward of the muzzle. For the steady jet, the position of the Mach disc relative to the muzzle for the steady jet is given as

$$x'_M/D = M_e\sqrt{\gamma_e \bar{p}_e/2}. \tag{11}$$

For this study, data are fitted for the source point position, $x_o = 0.375x'_M/D$, and for $x_o = 0$.

The values of the significant parameters are given in Table 2. The dependence of the momentum index, μ, is explored with these parameters.

The authors first used the approach given above on the data for distances $\geq$ 100 calibers. The blow-down parameter, β, was investigated because of the results obtained in Figure 3, which shows a different overpressure fall-off for different values of barrel length, or equivalently β. The scaled distance can be written in terms of some parameters of interest,

Table 2. Significant Blast Parameters

Designation	ℓ/D	δ	x'_M/D
c13p6	9.44	1.85	15.80
s220w9	4.95	18.10	7.07
s220w36	9.76	3.75	17.50
s125w42	10.70	2.39	22.20
l220w12	3.47	41.30	5.33
l125w12	3.66	23.00	6.40
l220w70	8.73	4.78	22.20
l125w75	10.29	3.60	25.80
105mm	13.84	0.85	37.25

$$r/\ell' = (r/D)(D/\ell)(\ell/\ell'_o)(\ell'_o/\ell'). \tag{12}$$

Here, ℓ'_o is the value that would be obtained using an infinitely long tube whereas ℓ' is the scale-length value that depends upon the field position for tubes of finite length. The behavior of ℓ' is assumed as

$$\frac{\ell'}{D} = \frac{\ell'_o}{D}\{1 - [1 - \exp(-B_1\bar{r})]\exp(-A_1\beta)\}, \tag{13}$$

in which $\beta = \delta\ell/\ell'$. For large distances, the scaled length would asymptotically approach the ratio of ℓ'/ℓ'_o corresponding to the blow-down parameter value. For small distances, the differences for long tubes and short tubes should diminish since the peak values would occur before the gun tube had emptied appreciably. The exponential term involving the distance is used to allow for this expected phenomenon.

3.2 Time of Arrival. As in Fansler and Schmidt (1983), the pressure-jump Mach relation,

$$\bar{P} = \frac{2\gamma}{\gamma+1}(M_s^2 - 1) \tag{14}$$

can be equated to the predictive equation for peak overpressure and integrated to obtain a closed form expression for the time of arrival, $\bar{t}_a$,

$$\bar{t}_a - \bar{t}_o = X(\bar{r}) - \frac{A'}{2} \ln [2X(\bar{r}) + 2\bar{r} + A'], \tag{15}$$

in which,

$$\bar{t} = \frac{t a_\infty}{\ell'} ,$$

$$X(\bar{r}) = \sqrt{\bar{r}^2 + A'\bar{r} + B'} ,$$

$$A' = \frac{2\gamma A}{\gamma + 1} , \qquad B' = \frac{2\gamma B}{\gamma + 1} ,$$

and γ is the specific heat ratio for ambient air. The quantity M_s is the Mach number for the shock front moving through the air.

3.3 Positive Phase Duration. The wave front travels at the speed determined by the peak overpressure of the wave. The point in the wave where the overpressure becomes zero travels at the speed of sound. The time for its arrival, $\bar{t}_c$, is

$$\bar{t}_c = \bar{r} + G. \tag{16}$$

Here G is a value that depends on other parameters, for instance, β. The positive phase duration is

$$\bar{\tau} = \bar{t}_c - \bar{t}_a, \tag{17}$$

or substituting in the expressions for $\bar{t}_a$ and $\bar{t}_c$,

$$\bar{\tau} = \bar{r} - X(\bar{r}) + \frac{A'}{2} \ln [2X(\bar{r}) + 2\bar{r} + A'] - \bar{t}_o + G. \tag{18}$$

The positive phase duration data will be used to find a form for G that will minimize the root mean square error.

3.4 Impulse. The impulse I is,

$$I = \int_{t_a}^{t_c} (p - P_\infty)\, dt. \tag{19}$$

The dimensionless form of the impulse is,

$$\bar{I} \equiv I a_\infty / (\ell' p_\infty). \tag{20}$$

A form for the impulse is sought that is consistent with the present treatments of the peak overpressure, time of arrival, and positive phase duration. The Friedlander waveform has been used successfully to describe the shape of the initial positive phase component of the wave for blasts (Baker 1973). The most primitive form is,

$$(p - P_\infty)/p_\infty = \bar{P}[1 - (t - t_a)/\tau] \exp[-(t - t_a)/\tau]. \tag{21}$$

Assuming the Friedlander relationship for the positive part of the waveform in Equation (19), we obtain the simple expression,

$$\bar{I} = \bar{P}\bar{\tau}/e. \tag{22}$$

To obtain a fit, we use the impulse data with the already fitted form of Equation (9) and with Equation (18), with G to be determined by least squares fitting of the impulse data.

4. RESULTS

4.1 Peak Overpressure. First, a fit was made to the far field data obtained at 100 and 400 calibers. The results of the fits with various parameters used are given in Table 3 in which A is the multiplying factor in Equation (9). At these distances, the contribution of the second term in Equation (9) is insignificant. The right-hand column gives the root mean square (rms) error for the fit.

The supposition that a source location in front of the muzzle improves the data fit contradicts our findings. However, other approaches are more successful. The rms error value is reduced when the momentum index, μ, is allowed to vary with Mach disc location. The use of ℓ/D as a parameter also provides good correlation. That both parameters provide good correlation is not surprising since the two parameters increase as the square root of the muzzle exit pressure.

The question whether ℓ' depends on β was investigated by fitting Equation (13) to the results of Model 10 in Table 3. The terms within the brackets approach unity in the far field and were set to unity in the fitting procedure. The parameter A_1 is an insensitive parameter for fitting and so the blow-down parameter was abandoned as a parameter to be used for any further fitting studies of the peak overpressure.

Table 3. Least Squares Fit Results for Far Field Peak Overpressure Data

Model	Momentum Index (μ)	A	Source Position	RMS
1	0.71	0.88	0.0	0.311
2	0.69	0.89	$0.375x'_M/D$	0.324
3	0.82	0.93	$b(0.375x'_M/D)$ b = -4.8	0.271
4	$a + b(\ell/D)$ $a = 0.91, b = -0.031$	0.90	$0.375x'_M/D$	0.270
5	$a + b(\ell/D)$ $a = 0.9, b = -.026$	0.90	0.0	0.267
6	$a + b(\ell/D) + c\delta$ $a = .88, b = -.028, c = .007$	0.90	$0.375x'_M/D$	0.271
7	$a + b(\ell/D) + c\delta$ $a = .87, b = -.023, c = .007$	0.90	0.0	0.268
8	$a + b\delta$ $a = .61, b = .0054$	0.89	$0.375x'_M/D$	0.281
9	$a + b\delta$ $a = .65, b = .0046$	0.90	0.0	0.275
10	$a + bx'_M/D$ $a = .87, b = -.01$	0.91	0.0	0.263
11	$a + b(x'_M/D)/M_e$ $a = .87, b = -.012$	0.91	0.0	0.267
12	$\ell'/\ell = ab\cos\theta + \sqrt{1 - a^2\sin^2\theta}$ $a = 0.31, b = 2.4$	0.76	0.0	0.287

A similar parameter study was performed with all the data. The results of the far field study were used to fix some of the parameters for some of the models. With these parameters fixed, the accuracy in the far field is emphasized at the expense of the predictions for the near field. Table 4 gives the value of μ together with the values of the multiplying factors, A and B, obtained with various approaches.

In addition, a fit was made to the data as in the previous work of Fansler and Schmidt (1983). With this set of data, the results were,

$$\bar{P} = 1.88\left(\frac{\ell'}{r}\right)^{1.2}, \tag{23}$$

in which $\mu = 0.72$. This compares with the old data fit of

$$\bar{P} = 2.4\left(\frac{\ell'}{r}\right)^{1.1}, \tag{24}$$

Table 4. Least Squares Fit Results for All Peak Overpressure Data

Model	Momentum Index (μ)	A	B	Source Position	RMS
1	0.7, Fixed	0.80	1.99	0.0	0.283
2	0.71	0.82	1.96	$0.375x'_M/D$	0.283
3	$a + b(\ell/D)$, Fixed $a = 0.91, b = -0.031$	0.88	1.50	$0.375x'_M/D$	0.354
4	$a + b(\ell/D)$ $a = 0.90, b = -0.026$	0.84	1.55	$0.375x'_M/D$	0.267
5	$a + b(\ell/D)$ $a = 0.81, b = -.019$	0.89	1.56	0.0	0.256
6	$a + b(x'_M/D)$ $a = .85, b = -.01$	0.83	1.57	$0.375x'_M/D$	0.260
7	$a + b(x'_M/D)$ $a = .83, b = -.0063$	0.89	1.61	0.0	0.249
8	$a + b(x'_M/D)/M_e$, Fixed $a = .86, b = -.012$	0.84	1.61	0.0	0.268
9	$a + b(x'_M/D)/M_e$ $a = .85, b = -.0086$	0.88	1.59	0.0	0.259

in which $\mu = 0.78$. The value of the momentum index is smaller for the new data and reflects the influence of the data in the far field in which the pressure differences with angle become less.

From this study, the predictive fit selected was model 7, where μ depends upon the Mach disc location. With A and B determined, the working version of Equation (9) can be written as,

$$\bar{P} = .89\left(\frac{\ell'}{r}\right) + 1.61\left(\frac{\ell'}{r}\right)^2, \tag{25}$$

in which

$$\mu = 0.83 - 0.0063(x'_M/D). \tag{26}$$

The result for μ shows that the ratio of the front to back shock strengths becomes lower with higher muzzle exit pressure. This result agrees with the data of Schomer and Raspet (1984). Predictions from Equation (25) are compared with the correlating data, as shown in Figure 4.

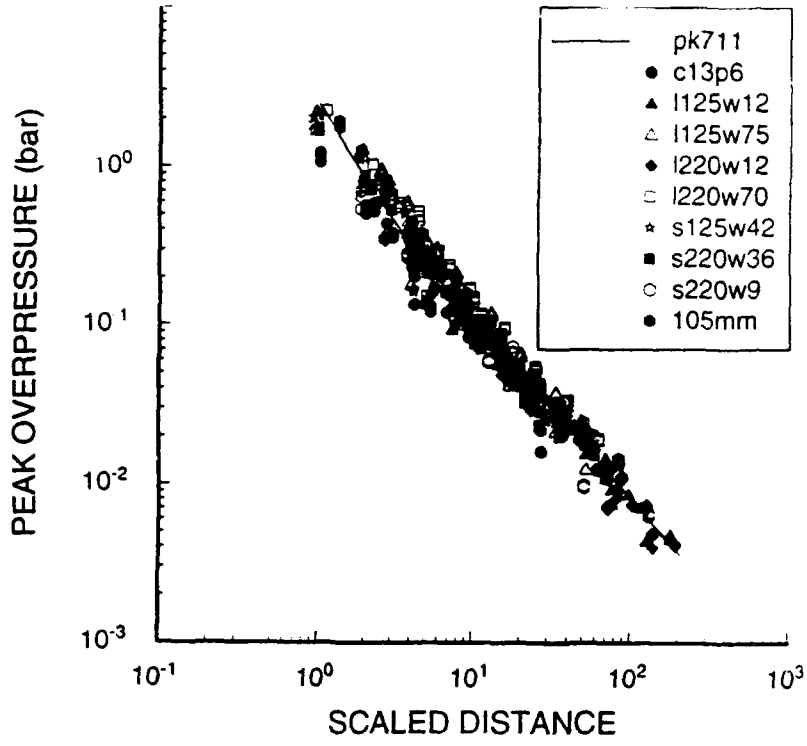

Figure 4. Pressure vs. Scaled Distance with New Approach

4.2 Time of Arrival. The time-of-arrival expression, Equation (15), can be used with the determined constants A and B and the time-of-arrival data to obtain,

$$\bar{t}_a = X(\bar{r}) - 0.52 \ln [2X(\bar{r}) + 2\bar{r} + 1.04] - 0.56, \tag{27}$$

in which,

$$X(\bar{r}) = \sqrt{\bar{r}^2 + 1.04\bar{r} + 1.88}\ .$$

The data were logarithmically weighted to minimize the relative error. The constants obtained with no weighting have comparable values. Least squares fits were also tried by re-determining the parameters previously found with the peak overpressure data. The obtained rms error was not improved significantly with the time-of-arrival data determining A, B, and μ.

Figure 5 shows the calculated $\bar{t}_a$ minus the observed $\bar{t}_a$ (residuals) as a function of the scaled length. Approximately 700 data points are shown in this graph. Most of the points are bunched, with a relatively few outlying data points scattered about. The time-of-arrival data were obtained with the aid of a code that determines automatically the peak overpressure, time of arrival, positive phase duration, and impulse. It is possible that some of the outlying

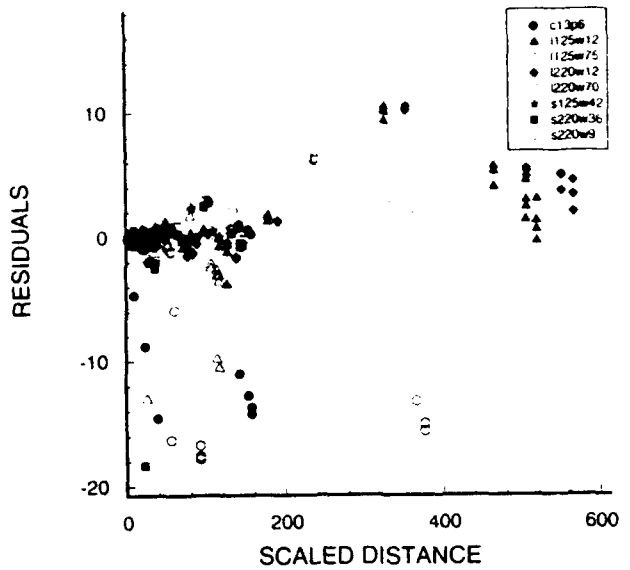

Figure 5. Calculated $\bar{t}_a$ Minus the Observed $\bar{t}_a$ (residuals) vs. r/ℓ'

data with negative values could be caused by triggering on the precursor. The origins of errors in the data have not yet been thoroughly investigated. Nevertheless, most of the data are densely located near the zero line except for the larger scaled distances. Another source of error is the uncertainty of the sound speed. The experiment was conducted covering a period from April to September, 1992, and significant differences in temperature (and thus sound speeds) could have occurred over the times when data were taken.

4.3 Positive Phase Duration. The positive phase duration data were obtained by using the code mentioned above. The code tests for the sign of the value of overpressure to change from positive to negative. This change in sign is also related to obtaining the impulse. If the sign changes and again goes positive within a given time interval and a significant amount of impulse is added, another sign change is needed to indicate that the positive phase of the wave has been completed. Various forms for G were assumed to find a minimum value for the rms error. Table 5 gives the forms tried and the results.

Table 5. Positive Phase Duration Parameter Fitting Results

Model	G	b_1	b_2	b_3	b_4	RMS
1	b_1	1.22				0.777
2	$b_1 - b_2 \cos\theta$	0.572	1.01			0.636
3	$b_1 + b_3[1 - \exp(-b_2\beta)] - b_4 \cos\theta$	- 0.157	.00264	16.8	8.14	0.620
4	$b_1 + b_2\beta - b_3 \cos\theta$	0.0944	0.0319	0.584		0.583

4.4 Impulse. As mentioned when discussing the positive phase duration results, a computer code developed to reduce the data has the capability to integrate the pressure data to obtain the impulse. It can also calculate the impulse for double peaks in quick succession, even though there might be a small interval in which the wave goes negative. For calculations of structural vulnerability the impulse is the important quantity. For our approach discussed earlier, $\bar{\tau}$ has to be determined in Equation (22). Equivalently for this approach, the value of G is determined.

The scaled impulse as a function of scaled distance is shown in Figure 6. The scatter is more pronounced than for the scaled peak overpressure. The two lower points were later eliminated as being processed improperly by the computer code.

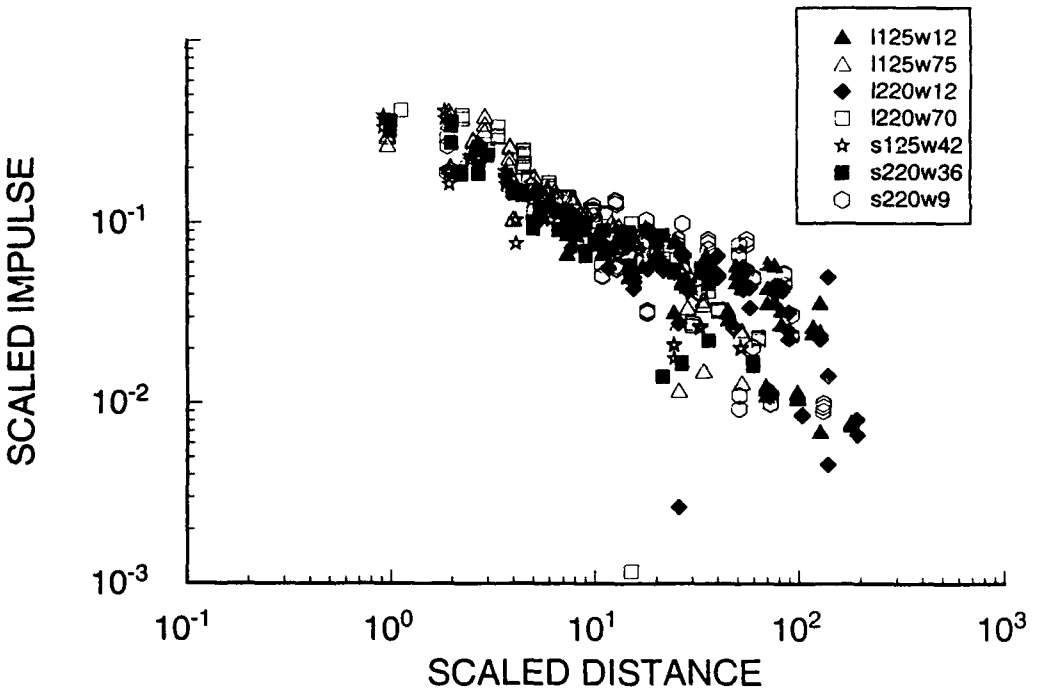

Figure 6. Scaled Impulse vs. Scaled Distance

Table 6 gives some of the models tried in terms of functions of G and the results. Model 19 is chosen to calculate the positive phase duration and, using Equation (25), the impulse. The value of G is,

$$G = 0.09 - 0.00379\delta + 1.07[1 - 1.36\exp(-0.049\bar{r})]\ell/\ell'. \tag{28}$$

Figure 7 shows the scaled impulse plotted with the predicted values for the firings that used the 220 grain projectile with 12 grains of powder for the long barrel (designated as l220w12). Figure 8 gives corresponding results for the s125w42 firings. These figures provide

Table 6. Impulse Parameter Results

Model	G	b_1	b_2	b_3	b_4	b_5	RMS
1	b_1	0.352					0.538
2	$b_1 + b_2\beta$	-.0649	0.0307				0.440
3	$b_1 + b_3\beta^{b_2}$	-.509	0.539	0.270			0.435
4	$b_1 + b_2\sqrt{\beta}$ $+b_3\beta$	-.488	0.261	0.0067			0.435
5	$b_1 + b_3\beta^{b_2}$ $-b_4\cos\theta$	0.134	0.972	0.0272	.455		0.418
6	$b_1 - b_2\cos\theta$	0.556	0.842				0.468
7	$b1 + b_2\beta$ $-b_3\cos\theta$	0.146	0.024	0.459			0.418
8	$b_1 + b_2\delta - b_3\cos\theta$	0.310	0.0276	0.744			0.450
9	$b_1 + b_3[1 - \exp(-b_2\beta)]$ $-b_4\cos\theta$	0.120	0.00298	9.39	0.446		0.417
10	$b_1 + b_2\beta$ $-b_3\cos\theta - b_4\beta\cos\theta$	0.160	0.0189	0.411	0.223		0.421
11	$b_1 + b_3[1 - \exp(-b_2\beta)]$	-.137	0.00781	5.78			0.438
12	$b_1 + b_2\sqrt{\delta} + b_3\ell/\ell'$	-.904	0.162	0.608			0.421
13	$b_1 + b_2\sqrt{\delta} + b_3\sqrt{\ell/\ell'}$	-1.75	0.174	1.49			0.428
14	$b_1 + b_2\delta + b_3\ell/\ell'$	-.680	0.193	0.619			0.425
15	$b_1 + b_2\beta + b_3\ell/\ell'$	-.486	0.0189	0.413			0.410
16	$b_1 + b_2(1 - \exp(-b_3\bar{r})$ $(1 - exp(-b_4\beta)$	-.100	4.179	0.0868	0.0179		0.424
17	$b_1 + b_2\beta[1 - \exp(-b_3\bar{r})]$ $(1 + b_4/\delta)$	-.268	0.0159	0.136	29.1		0.396
18	$b_1 + b_2\beta[1 - \exp(-b_3\bar{r})]$	-.0085	0.0337	0.108			0.433
19	$b_1 + b_2\delta$ $+b_3[1 - b_5\exp(-b_4\bar{r})]\ell/\ell')$	0.09	-0.00379	1.07	0.049	1.36	0.358

results from contrasting firing conditions. The l220w12 firings constitute firing from a long barrel with low velocities; the s125w42 firings constitute firing from a short barrel with high velocities. At the greater distances, the scaled impulse values are higher for the larger polar angles. Just the opposite behavior occurs at the smallest distances and the predictive curves reflect these trends also. We cannot, with certainty, explain these data trends. However, we speculate that the frontal part of the wave may be feeding energy around the positive phase of the wave to the rear of the gun.

A more careful analysis should also consider how the wave shape changes with distance and angle. Wilcoski and Pater (1990) show that the relative spectral frequency content of the wave changes significantly with distance. One could take this change into account with

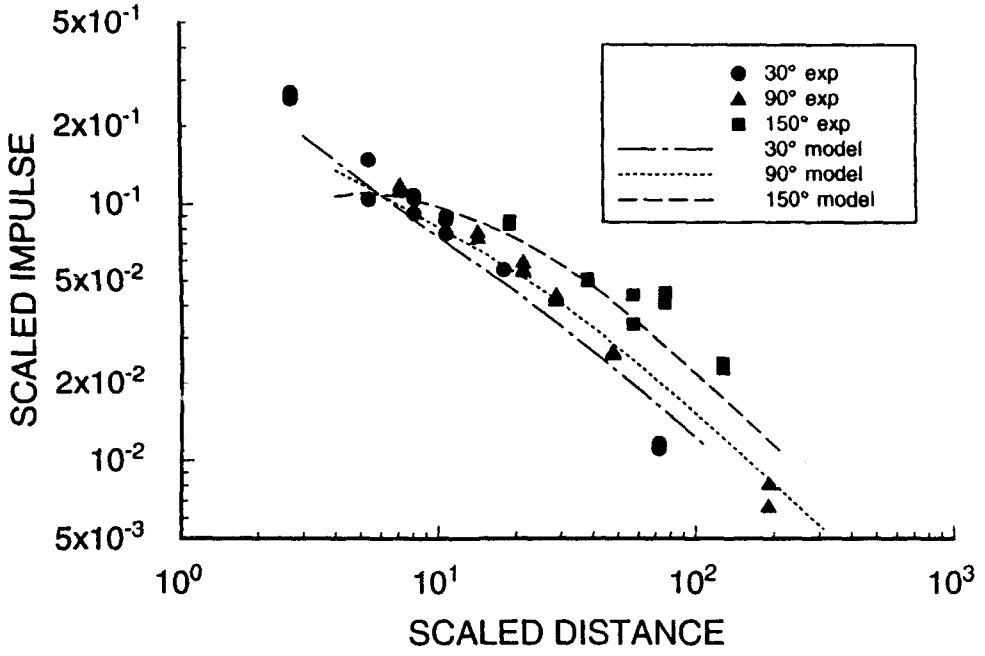

Figure 7. Comparison of Scaled Impulse with Predicted Values for l220w12 Firings

the use of the the modified Friedlander wave,

$$(p - P_\infty)/p_\infty = \bar{P}[1 - (t - t_a)/\tau] \exp[-h(t - t_a)/\tau]. \tag{29}$$

Here, h is the wave shape factor that varies with distance.

Data for instantaneous explosions (Baker 1973) show that the value of h declines with distance to a local minimum with a value near 2. Since the impulse is used more than the positive phase duration for structural computations, we have concentrated on getting a good fit to the impulse. For a constant value of impulse and peak overpressure, the normalized positive phase duration as a function of the wave shape factor, h, is shown in Figure 9. The positive phase duration is normalized by its value when $h = 1$. For our purposes, the assumption of $h = 1$ will only adversely affect the time representation of the directed wave and reflected waves that are close to each other.

4.5 Predictive Equations for the Far Field. If the peak overpressure described by Equation (25) is applied with the expression for the positive phase duration to the far-field, the symbolic and mathematical analysis package, Wolfram Research's *Mathematica* (1991), can be used to show that the energy in the blast wave has a logarithmic singularity at infinity. Clearly this result does not correspond to reality. Landau and Lifshitz (1959) show dissipation at large distances from the explosion results in the peak overpressure declining

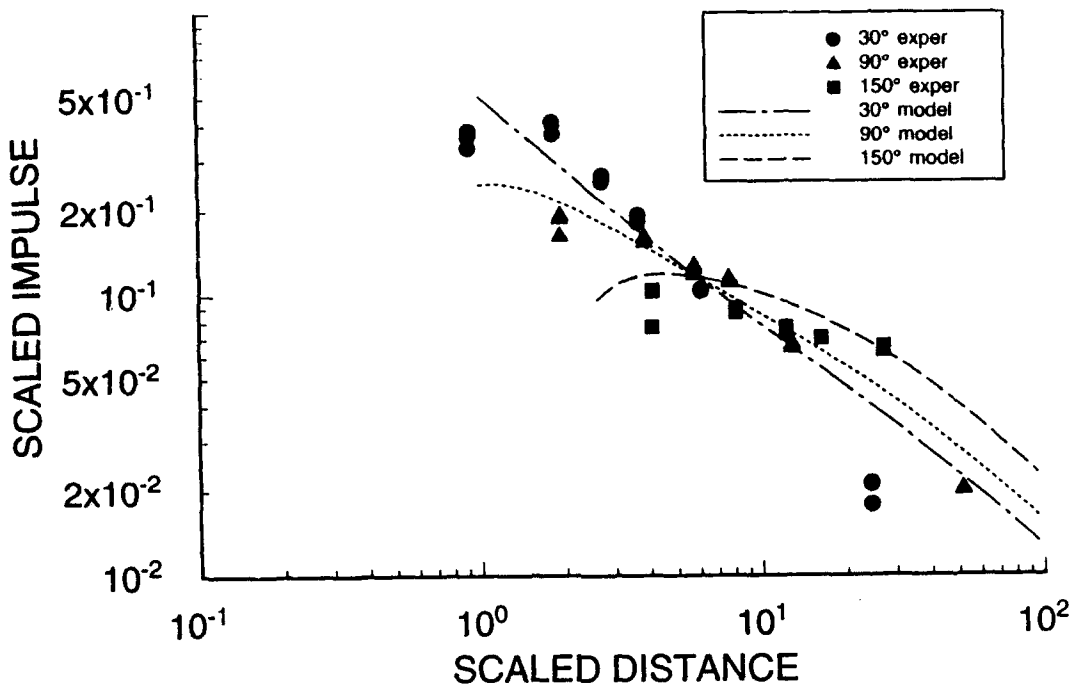

Figure 8. Comparison of Scaled Impulse with Predicted Values for s125w42 Firings

as,

$$\bar{P} = A_2/[\bar{r}\sqrt{\ln(\bar{r}/a_2)}]. \tag{30}$$

Using Equation (30), one can obtain $d\bar{t}/d\bar{r}$ as before and expand the result in series form for large $\bar{r}$. Integration to obtain the time of arrival and then the positive phase duration shows that the positive phase duration will grow as the square root of the log of the distance. The energy of the wave will then decline as the inverse square root of the distance. It was decided to match Equation (25) and Equation (30) at $\bar{r} = 50$. At this distance, the ratio of blast strengths for different angular positions is changing very slowly with distance and the wave behavior is almost linear as for an acoustical wave. With the slopes of the equations set equal to each other at this distance, the constants in Equation (30) give the particular working asymptotic form for the peak overpressure,

$$\bar{P} = 3.48975/[\bar{r}\sqrt{\ln(33119\bar{r})}]. \tag{31}$$

In turn the asymptotic form for the positive phase duration is also found and is,

$$\bar{\tau} = 2.99\sqrt{\ln(33119\bar{r})} - 8.534 + G. \tag{32}$$

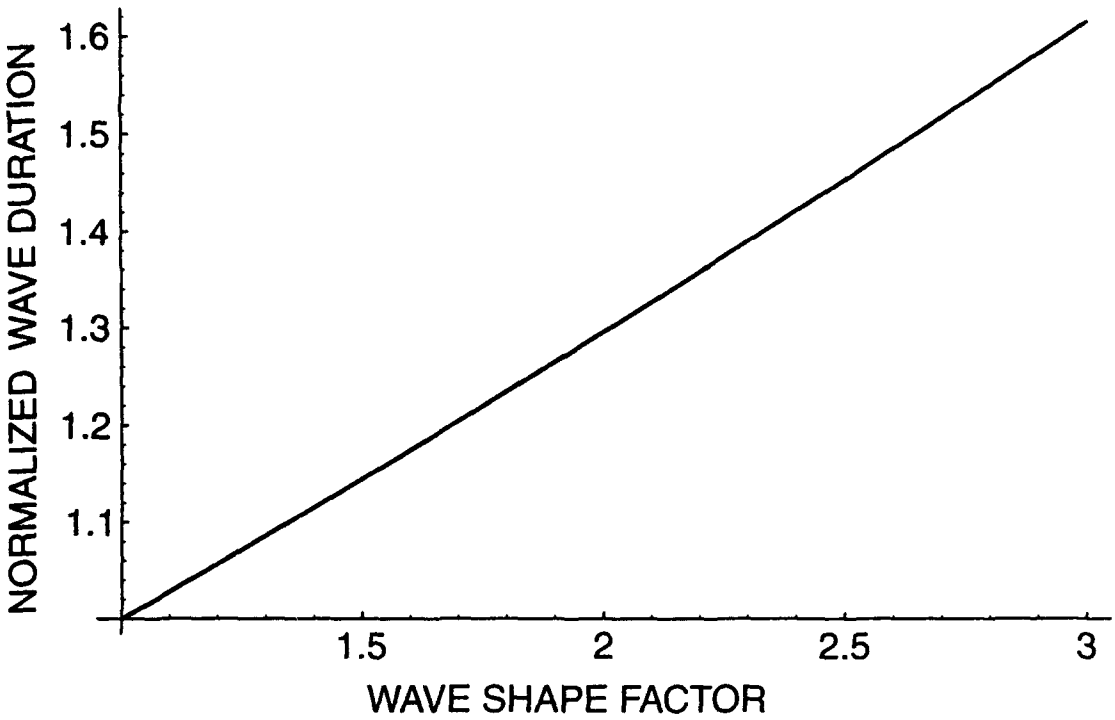

Figure 9. Normalized Positive Phase Duration vs. h, a Wave Shape Factor

Figure 10 shows a comparison of the asymptotic form for the duration, Equation (32), with the form from the least squares fit. Although the differences are small, only the asymptotic forms give the correct energy results in the limit of large distances.

With the complete solution now obtained, we can represent the positive phase duration as a function of scaled distance and angle, which is shown in Figure 11 . Although increasing comparatively rapidly at the smaller distances, the positive phase duration increases only slowly with larger distances. If data were taken only close to the weapon for a limited range of r, the scaled duration as a function of $\bar{r}$ would have its smallest values at small $\bar{r}$ and θ, and the largest values of τ would be found at a larger $\bar{r}$ and θ. The equivalent path over the surface in Figure 11 might approximate an almost linear relationship. Indeed, Fansler and Schmidt (1983) obtained such a linear fit.

4.6 Predictive Relationship for the Complete Wave. When waves are reflected from a surface, the direct wave and reflected wave will interact at some points in the field. The front of the reflected wave could also interact with the negative phase of the direct wave. To accurately predict the wave interaction, a knowledge of the negative phase is also needed. Formerly, the Reed wave description (1977) was used for both the positive and negative phase, but we have used the Friedlander description for the positive phase. The Friedlander wave is only descriptive of the positive phase. Thus, we need to join the Friedlander positive

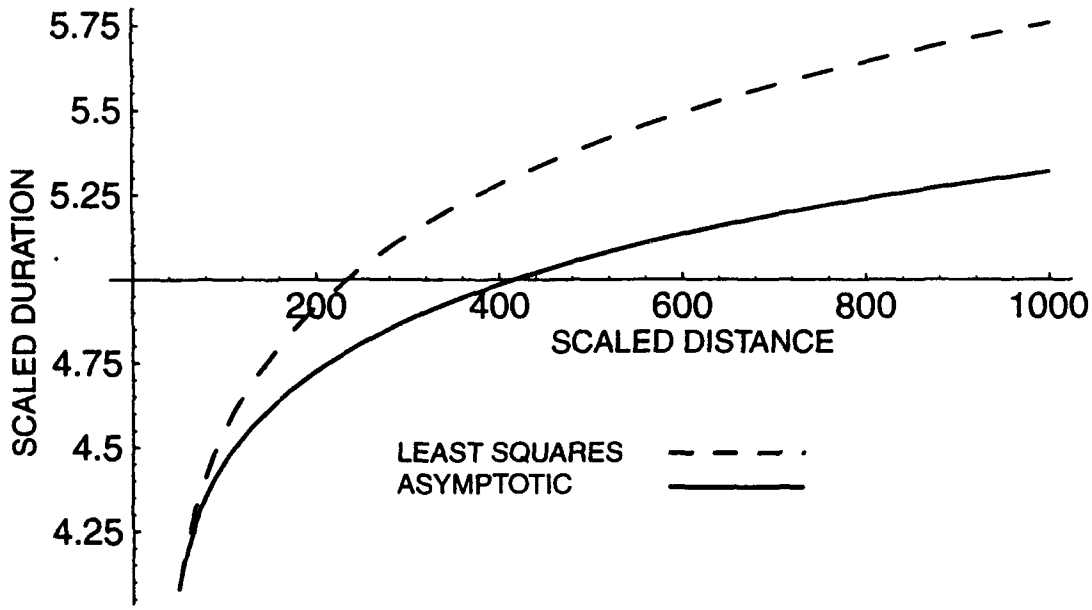

Figure 10. Parametric and Asymptotic Forms for the Positive Phase Duration

phase to the negative phase of the Reed description. The Reed wave is

$$(p - P_\infty)/p_\infty = \bar{P}[1 - (t - t_a)/\tau][1 - (t - t_a)/(3.67\tau)]\{1 - [(t - t_a)/(3.67\tau)]^2\}. \qquad (33)$$

For $t - t_a > \tau$, this equation multiplied by a factor to make the integral of the complete wave equal to zero describes the negative phase. If the time integral for the complete wave were not equal to zero, the total momentum of the wave would increase with distance with no limiting bound. The required factor is equal to 0.751. Figure 12 is a plot of the resulting wave. A discontinuity occurs at the juncture of the positive phase and the negative phase. The disparity in slope would be even greater if the shape factor, h, for the Friedlander wave were set equal to two, as one might prefer to optimally simulate the wave at larger distances.

4.7 Summary of Working Equations. These working equations are used to improve the present computer implementation for the muzzle blast (Heaps, Fansler, and Schmidt 1985). The peak overpressure for $\bar{r} < 50$ is,

$$\bar{P} = .89\left(\frac{\ell'}{r}\right) + 1.61\left(\frac{\ell'}{r}\right)^2 ,$$

in which the scaled length taking the polar angle from the boreline into account is,

$$\ell'/\ell = \mu\cos\theta + \sqrt{1 - \mu^2\sin^2\theta} ,$$

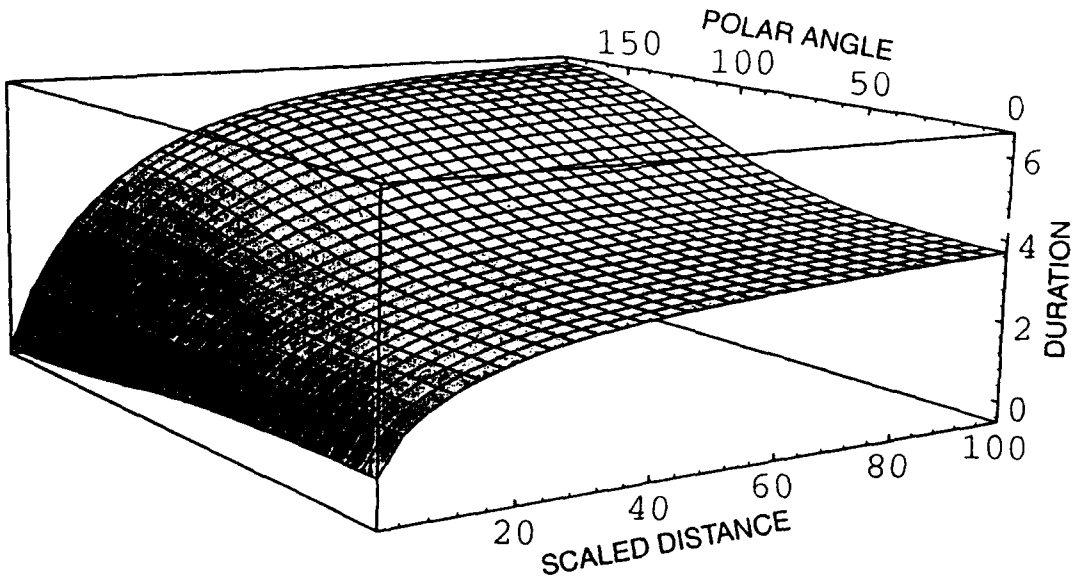

Figure 11. Scaled Positive Phase Duration vs. Scaled Distance and Angle

and μ, the momentum index is,

$$\mu = 0.83 - 0.0063(x'_M/D) \ .$$

The peak overpressure for $\bar{r} > 50$ is,

$$\bar{P} = 3.48975/[\bar{r}\sqrt{\ln(33119\bar{r})}].$$

The time of arrival is,

$$\bar{t}_a = X(\bar{r}) - 0.52\ln\left[2X(\bar{r}) + 2\bar{r} + 1.04\right] - 0.56 \ ,$$

in which,

$$X(\bar{r}) = \sqrt{\bar{r}^2 + 1.04\bar{r} + 1.88} \ .$$

The positive phase duration for $\bar{r} < 50$ is,

$$\bar{\tau} = \bar{r} - X(\bar{r}) + 0.52\ln\left[2X(\bar{r}) + 2\bar{r} + 1.04\right] + 0.56 + G \ ,$$

in which,

$$G = 0.09 - 0.00379\delta + 1.07[1 - 1.36\exp\left(-0.049\bar{r}\right)]\ell/\ell' \ .$$

The positive phase duration for $\bar{r} > 50$ is,

$$\bar{\tau} = 2.99\sqrt{\ln(33119\bar{r})} - 8.534 + G \ .$$

The expression for the impulse is,

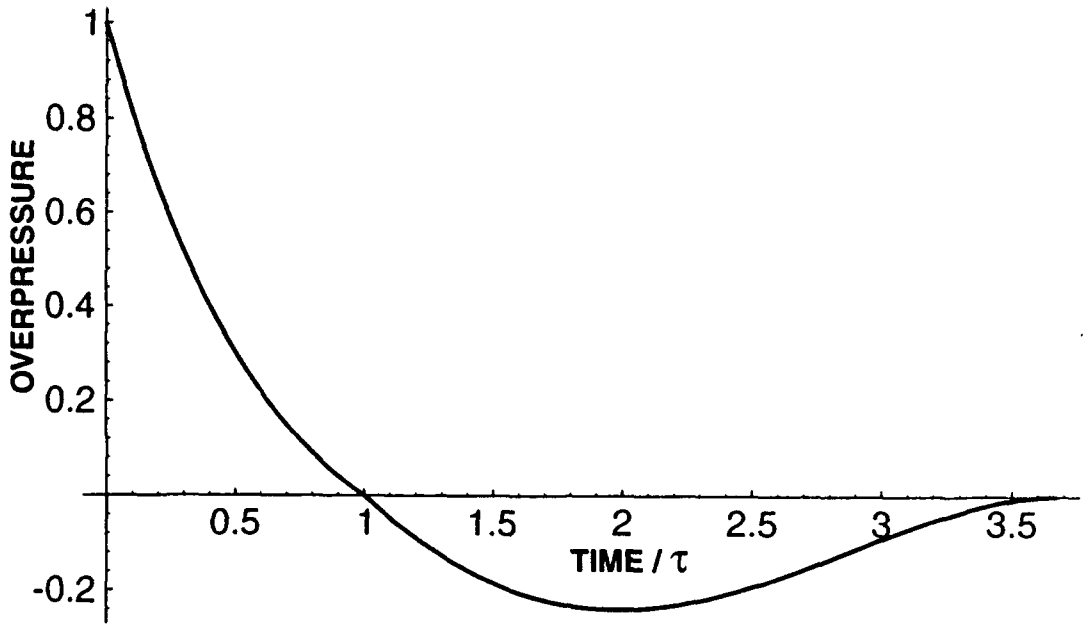

Figure 12. Pressure-Time Relationship for the Complete Wave

$$\bar{I} = \bar{P}\bar{\tau}/e \ ,$$

and the impulse can be determined from the above working equations. The overpressure-time relationship over the positive phase is,

$$(p - P_\infty)/p_\infty = \bar{P}[1 - (t - t_a)/\tau] \exp[-(t - t_a)/\tau] \ .$$

The overpressure-time relationship over the negative phase is,

$$(p - P_\infty)/p_\infty = 0.751\bar{P}[1 - (t - t_a)/\tau][1 - (t - t_a)/(3.67\tau)]\{1 - [(t - t_a)/(3.67\tau)]^2\} \ .$$

5. SUMMARY AND CONCLUSIONS

Overpressure data were obtained for a wide range of distances and angles from the muzzle. The data were then used in a parametric investigation to improve a predictive method based on dimensional analysis. In addition to the fundamental length scaling parameter, other parameters investigated were the Mach disc location and the blow-down parameter. Investigations in the far field showed that the blow-down parameter was, for the range of weapon parameters investigated, not a significant parameter for use in describing peak overpressure. Although the Mach disc location could not be used to improve the location of the source point, it was a meaningful parameter for helping to characterize the momentum index, μ. A two-term overpressure equation was assumed to take into account the nonlinear

blast wave near the muzzle. The new peak overpressure equation was used together with a result from gas dynamics to obtain a closed form expression for the time of arrival. Only one additional parameter needed to be determined by least squares fitting to obtain the predictive equation for time of arrival, whereas in the older model, two parameters were needed. The positive phase duration is constructed by subtracting the wave's time of arrival from the time for the wave's zero pressure point to arrive, assuming that this point travels at the speed of sound. A Friedlander wave is assumed with a value of the wave shape factor equal to one. With the assumed shape, the Friedlander wave is integrated to obtain the impulse. The impulse depends only upon the positive phase duration and the peak pressure. The free parameters assumed for the positive phase duration are then fitted to the impulse data.

For longer distances, a smooth join was made to the fitted pressure-distance curve with an inverse distance divided by the square root of the logarithm of the distance. The positive phase duration is also modified to grow with the square root of the logarithm of the distance. With these modifications, the total energy of the wave decays at long distances as the inverse square root of the logarithm of the distance. Although a physically valid solution is obtained at longer distances, use of this prediction method should be limited to distances where the wave does not extensively interact with noise-absorbing surfaces or is not subject to wave distortion by heterogeneous atmospheric conditions.

For detailed study of the interaction of the direct wave and the reflected wave, the negative phase of the wave is also needed. The Friedlander wave can give a good approximation over the positive phase of the wave but cannot describe the negative phase. To complete the wave, a modified description of the negative phase of a Reed wave is joined to a Friedlander wave. The negative phase of the wave conforms with the necessary condition that the time integral of a spherical wave equals zero, else the energy of the wave would grow with increasing distance.

Further work should include finding the wave shape factor as a function of scaled distance. The value of the impulse is not affected by errors in representing the wave shape but better prediction of wave interactions depends upon wave shape accuracy.

INTENTIONALLY LEFT BLANK.

6. REFERENCES

Baker, W. E. *Explosions in Air.* U. Texas Press, Austin, TX, 1973.

Erdos, J. I., and P. DelGuidice. "Gas Dynamics of Muzzle Blast." *AIAA Journal*, Vol. 13, pp. 1048-1055, August 1975.

Fansler, K. S., and E. M. Schmidt. "The Prediction of Gun Muzzle Blast Properties Utilizing Scaling." ARBRL-TR-02504, U.S. Army Ballistic Research Laboratory, Aberdeen Proving Ground, MD, July 1983. (AD B07859)

Fansler, K. S. "Dependence of Free Field Impulse on the Decay Time of Energy Efflux for a Jet Flow." *The Shock and Vibration Bulletin*, Part 1, The Shock and Vibration Center, Naval Research Laboratory, pp. 203-212, 22-24 October 1985.

Heaps, C. W.,, K. S. Fansler, and E. M. Schmidt. "Computer Implementation of a Muzzle Blast Prediction Technique." ARBRL-MR-3443, U.S. Army Ballistic Research Laboratory, Aberdeen Proving Ground, MD, May 1985. (AD A158344)

Kietzman, J.,, K. S. Fansler, and W. G. Thompson. "Muzzle Blast from 105mm M735 Round." ARBRL-MR-3957, U.S. Army Ballistic Research Laboratory, Aberdeen Proving Ground, MD, January 1992. (AD A245565)

Landau, L. D., and E. M. Lifshitz. *Fluid Mechanics.* Addison Wesley Publishing Co., Reading MA, 1959.

Pater, L. L. "Gun Blast Far Field Peak Overpressure Contours." TR 79-442, Naval Surface Weapons Center, Dahlgren, VA, March 1981.

Reed, J. W. "Atmospheric Attenuation of Explosion Waves." *Journal of the Acoustical Society of America*, Vol. 61, No. 1, pp. 39-47, January 1977.

Schomer, P. D.,, L. M. Little, and A. D. Hunt. "Acoustic Directivity Patterns for Army Weapons." Interim Report N-60, U. S. Army Construction Engineering Research Laboratory, Champaign, IL, January 1979.

Schomer, P. D., and R. Raspet. "Acoustic Directivity Patterns for Army Weapons – Supplement 2." Technical Report N-60, U. S. Army Construction Engineering Research Laboratory, Champaign, IL, August 1984.

Smith, F. "A Theoretical Model of the Blast from Stationary and Moving Guns." First International Symposium on Ballistics, Orlando, FL, 13-15 November 1974.

Soo Hoo, G., and G. R. Moore. "Scaling of Naval Gun Blast Peak Overpressures." TN-T7-72, Naval Surface Weapons Center, Dahlgren, VA, August 1972.

Wilcoski, J., and L. L. Pater. "Signal Analysis of Gun Muzzle Pressure Time Histories." *The Shock and Vibration Bulletin*, The Shock and Vibration Information Analysis Center, Booz-Allen and Hamilton Inc., Arlington, VA, October 1990.

Wolfram Research, Inc. *Mathematica.* Version 2, Wolfram Research, Inc., Champaign, IL, 1991.

INTENTIONALLY LEFT BLANK.

LIST OF SYMBOLS

A	parameter occurring in the expression for the peak overpressure
A_e	area of the bore (m/s)
B	parameter occurring in the expression for the peak overpressure
C	charge mass (kg)
D	bore diameter of gun (m)
E	energy of propellant at time of projectile ejection $(kg/m^2/s^2)$
G	parameter for determining time of arrival for zero overpressure
h	wave shape factor that varies with distance from muzzle
I	impulse for the positive phase of the wave
$\bar{I}$	nondimensionalized form of I, $\bar{I} = (Ia_\infty)/(\ell' p_\infty)$
ℓ	scale length for explosion (m)
ℓ'	effective scaling length that varies with angle from boreline $((m)$
ℓ'_o	value of length scale for gun tube of infinite length
L	tube length of gun (calibers)
m_p	mass of projectile (kg)
M_e	Mach number of propellant at muzzle after propellant ejection
M_s	Mach number for travelling shock of the blast
p_e	muzzle pressure for propellant after projectile ejection (Pa)
$\bar{p}_e$	nondimensionalized muzzle exit pressure, $\bar{p}/p_\infty$
p_∞	ambient pressure (Pa)
p_p	peak pressure at a field point (Pa)
P	peak overpressure, $p_p - p_\infty$ (Pa)

$\bar{P}$	dimensionless peak overpressure, P/p_∞
r	distance from muzzle
$\bar{r}$	nondimensionalized distance from muzzle, r/ℓ'
t	time after projectile uncorks (s)
t_a	blast wave time of arrival (s)
$\bar{t}_a$	nondimensionalized time of arrival, $t_a a_\infty/\ell'$
$\bar{t}_o$	integrating constant for time-of-arrival expression
V_p	exit velocity of projectile
x'_M	position of the Mach disc for steady jet conditions (m)
x_o	source point position investigated for improving prediction model
X	function of r defined for convenience in time-of-arrival expression
β	blow-down parameter with angle taken into account, $\beta = \delta\ell/\ell'$
δ	blow-down parameter, $\delta = (La_\infty)/(V_p\ell)$
γ	specific heat ratio
γ_e	specific heat ratio for exiting propellant gas
θ	polar angle from gun boreline
μ	momentum index, controls directivity of the blast
ρ_∞	ambient density (kg/m^3)
τ	positive phase duration for the blast wave (s)
$\bar{\tau}$	nondimensionalized positive phase duration, $\tau a_\infty/\ell'$
e	exit conditions
m	muzzle conditions immediately before uncorking
∞	ambient conditions

No. of Copies	Organization
2	Administrator Defense Technical Info Center ATTN: DTIC-DDA Cameron Station Alexandria, VA 22304-6145
1	Commander U.S. Army Materiel Command ATTN: AMCAM 5001 Eisenhower Ave. Alexandria, VA 22333-0001
1	Director U.S. Army Research Laboratory ATTN: AMSRL-OP-CI-AD, Tech Publishing 2800 Powder Mill Rd. Adelphi, MD 20783-1145
1	Director U.S. Army Research Laboratory ATTN: AMSRL-OP-CI-AD, Records Management 2800 Powder Mill Rd. Adelphi, MD 20783-1145
2	Commander U.S. Army Armament Research, Development, and Engineering Center ATTN: SMCAR-IMI-I Picatinny Arsenal, NJ 07806-5000
2	Commander U.S. Army Armament Research, Development, and Engineering Center ATTN: SMCAR-TDC Picatinny Arsenal, NJ 07806-5000
1	Director Benet Weapons Laboratory U.S. Army Armament Research, Development, and Engineering Center ATTN: SMCAR-CCB-TL Watervliet, NY 12189-4050
1	Director U.S. Army Advanced Systems Research and Analysis Office (ATCOM) ATTN: AMSAT-R-NR, M/S 219-1 Ames Research Center Moffett Field, CA 94035-1000

No. of Copies	Organization
1	Commander U.S. Army Missile Command ATTN: AMSMI-RD-CS-R (DOC) Redstone Arsenal, AL 35898-5010
1	Commander U.S. Army Tank-Automotive Command ATTN: AMSTA-JSK (Armor Eng. Br.) Warren, MI 48397-5000
1	Director U.S. Army TRADOC Analysis Command ATTN: ATRC-WSR White Sands Missile Range, NM 88002-5502
(Class. only) 1	Commandant U.S. Army Infantry School ATTN: ATSH-CD (Security Mgr.) Fort Benning, GA 31905-5660
(Unclass. only) 1	Commandant U.S. Army Infantry School ATTN: ATSH-WCB-O Fort Benning, GA 31905-5000
1	WL/MNOI Eglin AFB, FL 32542-5000
	Aberdeen Proving Ground
2	Dir, USAMSAA ATTN: AMXSY-D AMXSY-MP, H. Cohen
1	Cdr, USATECOM ATTN: AMSTE-TC
1	Dir, ERDEC ATTN: SCBRD-RT
1	Cdr, CBDA ATTN: AMSCB-CII
1	Dir, USARL ATTN: AMSRL-SL-I
10	Dir, USARL ATTN: AMSRL-OP-CI-B (Tech Lib)

No. of Copies	Organization
1	Commander US Army Armament, Munitions and Chemical Command ATTN: AMSMC-LEP-L Rock Island, IL 61299-5000
1	Director US Army Missile & Space Intelligence Center ATTN: AIAMS-YDL Redstone Arsenal, AL 35898-5000
3	Commander US Army Watervliet Arsenal ATTN: SMCWV-QAR, T. McCloskey SMCWV-ODW, T. Fitzpatrick SMCWV-ODP, G. Yarter Watervliet, NY 12189
6	Commander US Army Armament RD&E Center ATTN: SMCAR-FS, Dr. Davidson SMCAR-CC, Mr. Hirshman SMCAR-CCH, Mr. Moore SMCAR-CCL, Mr. Johnson E. Seeling J. Donham Picatinny Arsenal, NJ 07801-5000
2	Commander US Army Tank Automotive Command ATTN: AMCPM-BFVS ATTN: AMCPM-BFVS-SC, K. Pitco Warren, MI 48397-5000
1	Commander US Army Missile Command ATTN: AMSMI-RD, Dr. W. Walker Redstone Arsenal, AL 35898-5000
1	Commander Tank Main Armament Systems ATTN: AMCPM-TMA, R. Billington Picatinny Arsenal, NJ 07806-5000
2	Commandant US Army Infantry School ATTN: ATSH-IV-SD, R. Gorday ATSH-TSM Fort Benning, GA 31905-5660
6	Director Benet Weapons Laboratory U. S. Armament Research, Development, and Engineering Center ATTN: SMCAR-CCB, J. Bendick T. Simkins SMCAR-CCB-DS, P. Vottis SMCAR-CCB-DS, C. Andrade SMCAR-CCB-RA, G. Carofano SMCAR-CCB-RA Watervliet, NY 12189-4050
1	Commander Army Research Office ATTN: AMXRO-MCS, Mr. K. Clark P.O. Box 12211 Research Triangle Park, NC 27709-2211
1	Commander Army Research Office ATTN: AMXRO-RT-IP, Library Services P.O. Box 12211 Research Triangle Park, NC 27709-2211
1	Commander Aviation Applied Technical Dir. ATTN: SAVRT-TY-MSMA, G. Moffatt Fort Eustis, VA 23604-5577
3	Department of the Army Construction Engineering Research Laboratory ATTN: CERL-SOI, P. Schomer L. Pater J. Wilcoski P. O. Box 4000 Champaign, IL 61820
1	Commander ASD/YHT ATTN: LT J. Palumbo D. Curley Eglin AFB, FL 32542
1	Commander (Code 3433) Naval Warfare Center ATTN: Tech Lib China Lake, CA 93555

No. of Copies	Organization
2	Commander Naval Surface Warfare Center ATTN: 6X, J. Yagla G. Moore Dahlgren, VA 22448
1	Commander (Code 6120C) Naval Ordnance Station ATTN: Susan Peters Indian Head, MD 20640
1	Commander US Naval Air Systems Command ATTN: AIR-604 Washington, DC 20360
1	Commander (Code 3892) Naval Warfare Center ATTN: K. Schadow China Lake, CA 93555
1	Commander (Code 730) Naval Surface Weapons Center Silver Spring, MD 20910
1	Director NASA Scientific & Technical Information Facility ATTN: SAK/DL P. O. Box 8757 Baltimore/Washington International Airport, MD 21240
1	McDonnell Douglas ATTN: Joseph Smuckler 1014 Ferngate Lane Creve Coeur, MO 63141
2	Alliant Techsystems Inc. ATTN: MS MN 50-2060, T. Melanger S. Langley 600 Second Street, Northeast Hopkins, MN 55343
1	S & D Dynamics, Inc. ATTN: R. Becker 7208 Montrico Dr Boca Raton, FL 33433-6930

No. of Copies	Organization
2	AAI Corporation ATTN: T. Stasney J. Hebert P. O. Box 126, MS 100-405 Hunt Valley, MD 21030-0126
2	Aerojet General Corporation ATTN: W. Wolterman A. Flatau P. O. Box 296 Azusa, CA 91702
1	Lockheed Aircraft, Inc. ATTN: J. Brown J. Perez P. O. Box 33, Dept. 1-330/UPLAND Ontario, CA 91761
1	General Electric Armament & Electric Systems ATTN: R. Whyte Lakeside Avenue Burlington, VT 05401
1	Franklin Institute ATTN: Tech Library Race & 20th Streets Philadelphia, PA 19103
1	Director Applied Physics Laboratory The Johns Hopkins University Johns Hopkins Road Laurel, MD 20707
2	Loral Corporation ATTN: S. Schmotolocha B. Axely 300 N. Halstead St. P. O. Box 7101 Pasadena, CA 91109
2	McDonnell Douglas Helicopter Co. ATTN: D. Van Osteen R. Waterfield Mail Station D216 500 E. McDowell Rd. Mesa, AZ 85205

No. of Copies	Organization
1	FN Manufacturing, Inc. ATTN: George Kontis Post Office Box 24257 Columbia, SC 29224
1	Red Eye Arms, Inc. ATTN: David Byron Gunn Station 507 N. New York Ave. Winter Park, FL 32789
1	Old Dominion University Mathematics Department ATTN: Dr. Charlie Cooke Norfolk, VA 23508
1	Scitec Inc. ATTN: Alex Zislan 100 Wall Street Princeton, NJ 08540
1	Los Alamos National Lab. ATTN: Thomas Davis Group WX-4 MS G787 Los Alamos, NM 87545
1	Olin Corporation ATTN: Stephan Faintich PO Box 222 St. Marks, FL 32355
1	Atlantic Research Corp. ATTN: Mark Friedlander 5945 Wellington Road MS G787 Gainesville, VA 22065

No. of Copies	Organization
	Aberdeen Proving Ground
2	Dir, USAMSAA ATTN: AMXSY-D, Mr. W. Brooks Mr. R. Conroy
7	Cdr, USACSTA ATTN: STECS-TD, Mr. Kelton STECS-AAL, M. Maule STECS-AA-LA, J. Scheuren STECS-AS-LA, S. Walton STECS-DA, P. Paules STECS-RM-PF, S. Hinte STECS-AS-HP, J. Andrews
2	Cdr, USATECOM ATTN: AMSTE-TE-R, Mr. Keele AMSTE-TA-R, W. Marshall
1	Dir, AMC Int. Mat. Eval. Div. ATTN: AMCICP-IM, R. Bloom
2	Dir, USARL ATTN: AMSRL-HR-SD, G. Garinther J. Kalb

USER EVALUATION SHEET/CHANGE OF ADDRESS

This Laboratory undertakes a continuing effort to improve the quality of the reports it publishes. Your comments/answers to the items/questions below will aid us in our efforts.

1. ARL Report Number ARL-TR-227 Date of Report September 1993

2. Date Report Received _____

3. Does this report satisfy a need? (Comment on purpose, related project, or other area of interest for which the report will be used.) _____

4. Specifically, how is the report being used? (Information source, design data, procedure, source of ideas, etc.) _____

5. Has the information in this report led to any quantitative savings as far as man-hours or dollars saved, operating costs avoided, or efficiencies achieved, etc? If so, please elaborate. _____

6. General Comments. What do you think should be changed to improve future reports? (Indicate changes to organization, technical content, format, etc.) _____

CURRENT ADDRESS

_____
Organization

_____
Name

_____
Street or P.O. Box No.

_____
City, State, Zip Code

7. If indicating a Change of Address or Address Correction, please provide the Current or Correct address above and the Old or Incorrect address below.

OLD ADDRESS

_____
Organization

_____
Name

_____
Street or P.O. Box No.

_____
City, State, Zip Code

(Remove this sheet, fold as indicated, tape closed, and mail.)
(DO NOT STAPLE)

DEPARTMENT OF THE ARMY

OFFICIAL BUSINESS

BUSINESS REPLY MAIL
FIRST CLASS PERMIT No 0001, APG, MD

Postage will be paid by addressee

Director
U.S. Army Research Laboratory
ATTN: AMSRL-OP-CI-B (Tech Lib)
Aberdeen Proving Ground, MD 21005-5066

NO POSTAGE
NECESSARY
IF MAILED
IN THE
UNITED STATES